Phonon density of states in R_2CuO_4 and superconducting $R_{1.85}Ce_{0.15}CuO_4$ (R =Nd,Pr)

I. W. Sumarlin and J. W. Lynn
Department of Physics, Center for Superconductivity Research, University of Maryland, College Park, Maryland 20742 and Reactor Radiation Division, National Institute of Standards and Technology, Gaithersburg, Maryland 20899

D. A. Neumann and J. J. Rush
Reactor Radiation Division, National Institute of Standards and Technology, Gaithersburg, Maryland 20899

C-K. Loong
Intense Pulsed Neutron Source, Argonne National Laboratory, Argonne, Illinois 60439

J. L. Peng and Z. Y. Li
Center for Superconductivity Research, Department of Physics, University of Maryland, College Park, Maryland 20742
(Received 13 November 1992)

Inelastic-neutron-scattering measurements of the generalized phonon density of states (GDOS) for the electron-doped superconductors $Nd_{1.85}Ce_{0.15}CuO_4$ and $Pr_{1.85}Ce_{0.15}CuO_4$ have been carried out with the use of both a filter-detector method and time-of-flight spectroscopy. A measurement of the GDOS for the insulating Pr_2CuO_4 was also done for comparison with that of $Pr_{1.85}Ce_{0.15}CuO_4$, while a more limited set of data was obtained for Nd_2CuO_4. Comparison between the GDOS spectrum of the $Nd_{1.85}Ce_{0.15}CuO_4$ with that of $Pr_{1.85}Ce_{0.15}CuO_4$ shows differences in the shape of some structures in the GDOS spectrum. Furthermore, there are substantial changes in the GDOS spectrum of $Pr_{1.85}Ce_{0.15}CuO_4$ as compared to that of Pr_2CuO_4, particularly in the energy regime between 33 and 63 meV. In the $Nd_{1.85}Ce_{0.15}CuO_4$ system, where electron-tunneling measurements have been performed, there are similarities between the GDOS spectrum and the Eliashberg-coupling function $\alpha^2F(\omega)$ obtained from the tunneling data in the energy regions where comparisons can be made. To the extent that this comparison is valid, it suggests that phonons are to some extent involved in the electron-pairing mechanism in these electron-doped superconductor systems. We have also determined the ground-state crystal-field excitations associated with the rare-earth ions (Nd^{3+}, Pr^{3+}). The Nd^{3+} crystal-field levels are observed at energies of 13, 20.7, 26.4, and 93 meV in superconducting $Nd_{1.85}Ce_{0.15}CuO_4$. For the Pr_2CuO_4 system, the Pr^{3+} crystal-field excitations are found at 18.6 and 87.9 meV. These peaks broaden and split when doped to form superconducting $Pr_{1.85}Ce_{0.15}CuO_4$. The observed crystal-field levels in the above systems are in good agreement with those reported by other groups.

I. INTRODUCTION

The role of phonons in the mechanism of superconductivity for the high-T_c oxide superconductors[1] is still largely an open issue. Historically, one indication for the electron-phonon mechanism in conventional superconductors has been the isotope effect[2] ($T_c \propto M^{-\alpha}$), where the BCS value for the isotope exponent is $\alpha=\frac{1}{2}$. For the copper-oxide superconductors, the oxygen exponent α has been found to depend on the carrier concentration and T_c.[3] In fact, for hole-doped superconductors the value of α has a decreasing trend with increasing T_c and with increasing number of CuO layers, n, with the exception of $YBa_{2-x}Sr_xCu_3O_7$.[3] In the electron-doped superconductors such as $Nd_{1.85}Ce_{0.15}CuO_4$ ($T_c \cong 25$ K),[4] α has been found to be very small ($\alpha \leq 0.05$).[5] The absence of an isotope effect by itself, of course, does not rule out a phonon-mediated pairing mechanism.[6] Indeed, there is substantial evidence from inelastic neutron scattering that the phonons are involved in the superconducting state, both in the present moderate-T_c electron superconductors,[7] as well as the high-T_c materials $YBa_2Cu_3O_7$ (Ref. 8) and $Bi_2Sr_2CaCu_2O_8$.[9]

One of the most direct experimental probes of the electron-phonon coupling in superconductors is a comparison of the electron-phonon spectral function $\alpha^2F(\omega)$ determined by electron-tunneling measurements with phonon density-of-states spectra measured by neutron scattering.[2,10] This approach has been used in the $Ba_{1-x}K_xBiO_3$ system[11] ($T_c \cong 30$ K, $\alpha=0.41$),[12] where reasonably good agreement was found between the tunneling and neutron data.[13] Electron-tunneling measurements have also been made on single crystals of $Nd_{1.85}Ce_{0.15}CuO_4$ grown in our laboratory,[11] and as a result we embarked on a determination of the phonon density of states in these systems to compare with the tunneling data.[7] We have measured the generalized phonon density of states (GDOS) on polycrystalline samples of superconducting $Nd_{1.85}Ce_{0.15}CuO_4$ and $Pr_{1.85}Ce_{0.15}CuO_4$, as well as on insulating Pr_2CuO_4. We have also obtained a limited set of data for Nd_2CuO_4. For the $Nd_{1.85}Ce_{0.15}CuO_4$ material where tunneling data have

0163-1829/93/48(1)/473(10)/$06.00

been obtained, we find that there are indeed some similarities between the two sets of data. Of course, in the anisotropic copper-oxide systems tunneling experiments accurate enough to extract $\alpha^2F(\omega)$ are generally very difficult to perform due to the short coherence lengths,[10] and any observed similarities between $\alpha^2F(\omega)$ and the GDOS have to be viewed with some reservations. Measurements of the phonon density of states, on the other hand, are less difficult to make, although in the present systems separating the magnetic (crystal-field) excitations from phonon scattering also presents some challenges. Nevertheless, the present GDOS measurements should serve for comparison purposes as more refined tunneling data become available.

In principle, there are two methods to determine the phonon density of states via inelastic neutron scattering. One method is to make extensive measurements of the phonon dispersion relations, generally along high-symmetry directions in reciprocal space, at as many reduced wave vectors as possible. Large, high-quality single crystals, of both the parent insulating systems and the doped superconducting materials, are needed for these types of measurements. Ideally, these measurements can then be compared with model calculations of the dispersion relations, and the model parameters are then adjusted to achieve a reasonable description of the dispersion relations. The model is then used to obtain an estimate of the phonon density of states. However, in the present systems where there are many phonon modes (21 in the present case), the model calculations play a much more important role in that they generally must be used to assign each measured phonon group to a specific phonon dispersion relation. The phonon energy and intensity information is then fed back into the model to make new predictions, and this type of iterative process is used to both conduct measurements and interpret data. Generally, this is not a straightforward procedure, and moreover the model must be simplified for calculational purposes. In the final analysis there are typically significant discrepancies between the calculated and observed energies along the high-symmetry directions.[14,15] To accurately calculate the phonon density of states, however, one must rely on the model to generate the correct phonon energies at all q values, not only along the high-symmetry directions, but also throughout the Brillouin zone. In the case of the doped $Nd_{1.85}Ce_{0.15}CuO_4$ and $Pr_{1.85}Ce_{0.15}CuO_4$ alloys of primary interest, it is not clear how well the partial, random substitution of Nd by Ce can be modeled by lattice dynamical calculations. Therefore the reliability of the density of states obtained with this method is difficult to assess in these complicated materials.

The second method is to directly measure the generalized phonon density of states via inelastic neutron scattering from polycrystalline materials, which has the distinct advantage that a model-independent determination can be made. For a single-component system (such as Pb), a measurement of the GDOS would in fact reflect the true phonon density of states. In a multicomponent system such as the present materials, on the other hand, this method has the drawback that the data are weighted by (σ_i/m_i), where σ_i is the nuclear scattering cross section and m_i is the mass of the ith ion, hence the term "generalized" phonon density of states. It is important to keep in mind when comparing the tunneling and neutron data that in fact neither technique directly measures the phonon density of states $F(\omega)$; the tunneling data are weighted by the electron-phonon coupling α^2. Hence, for these multicomponent oxide systems, we cannot expect the detailed correspondence that can be obtained for simple systems such as lead.

The presence of magnetic rare-earth ions (Nd^{3+},Pr^{3+}) in these electron-superconductor systems and the magnetic Cu^{2+} spins means that there are also magnetic contributions to the scattering.[16–19] The rare-earth spins order at very low temperatures ($T_N \lesssim 2$ K),[16,17] while the Cu spins order at high temperatures ($T_N \sim 250$ K) in the insulating compounds.[17–19] In the present materials the Cu ions have a small moment and thus scatter weakly. Moreover, this magnetic scattering is spread over a wide range in energy,[20] and indeed it is the large energy scale associated with this magnetism that has supported the speculation that it is directly connected with Cooper pairing. It is unlikely that the inelastic magnetic scattering from the Cu spins can be observed at all in these polycrystalline samples—single crystals are required to observe this.

The rare-earth–rare-earth interactions, on the other hand, are very weak, giving rise to ordering temperatures of a few degrees K or less. Hence the crystal-field excitations have little dispersion and thus give rise to sharp, Q-independent peaks in the inelastic spectra. Most of these peaks are very strong due to the large rare-earth moments and are easily identified. We note that the crystal-field excitations we have observed are in good agreement with those reported by other groups,[21–23] but in some cases we have been able to take data with better resolution than previous measurements. At the energies where these crystal-field excitations occur, however, it is not possible to separate the magnetic from phonon scattering. Furthermore, at elevated temperatures additional crystal-field transitions can be observed via the thermal population of excited states, while the crystal-field transitions tend to broaden. This makes temperature-dependent measurements of the GDOS very difficult. Fortunately, the temperature region of interest is at and below T_c (~ 25 K), and consequently we have restricted our measurements to low temperatures. We note that preliminary reports of our measurements have already been presented.[7,24]

II. EXPERIMENTAL PROCEDURES

For coherent scatterers with vibrational energy $\hbar\omega$, the one-phonon cross section in the incoherent approximation is given by[25]

$$\frac{d^2\sigma}{d\Omega\, d\omega} \propto \frac{k_f}{k_i} S(Q,\omega) , \tag{1}$$

with

$$S(Q,\omega)=\sum_j \frac{c_j\sigma_j}{m_j}\langle(\mathbf{Q}\cdot\mathbf{e}_j)^2 e^{-W_j(Q)}\rangle\frac{n(\omega)+1}{\omega}F_j(\omega)\ , \tag{2}$$

where c_j, σ_j, m_j, $\mathbf{e}_j$, $W_j(Q)$, and F_j are the concentration, total coherent scattering cross section, mass, phonon unit-polarization vector, Debye-Waller factor, and density of states, respectively, for the jth atom. $\mathbf{k}_i$ and $\mathbf{k}_f$ are the incident and final neutron wave vectors, $\hbar\mathbf{Q}$ is the momentum transfer, and $n(\omega)$ is the Bose thermal occupational factor. At low temperatures the thermal factor $n(\omega)+1\simeq 1$, and the effect by the Debye-Waller factor is assumed to be small for each ion. The quantity within the angular bracket $\langle\cdots\rangle$ is averaged over all modes with energy $\hbar\omega$, and this also includes averaging over all $\mathbf{Q}$ directions for polycrystalline materials. The above equation contains the generalized phonon density of states ρ

$$\rho=\sum_j \frac{c_j\sigma_j}{m_j}\langle(\hat{\mathbf{Q}}\cdot\mathbf{e}_j)^2 e^{-W_j}\rangle F_j(\omega)\ . \tag{3}$$

The incoherent approximation is best realized under experimental conditions with large values of Q. However, for moderate Q values, it has been shown that a reliable GDOS can be obtained by averaging over a range of scattering angles.[26] The contribution to the GDOS from each $F_j(\omega)$ is weighted mainly by σ_j/m_j, which for Nd, Pr, Ce, Cu, and O are, respectively, 0.11, 0.15, 0.02, 0.12, and 0.26 b/amu. The phonon cross sections are therefore particularly sensitive to scattering from oxygen vibrations.

The main technique we used to measure the GDOS is the filter-detector technique. These data were collected at the BT-4 spectrometer at the National Institute of Standards and Technology Research Reactor. The primary experimental advantage of this technique is that it provides excellent signal to noise while maintaining good energy resolution. The technique employs a thick polycrystalline block of Be in front of the detector, which transmits only neutrons with a final energy $E_f\lesssim 5$ meV. The scattering intensity as a function of energy is then obtained by varying the incident neutron energy. Improved energy resolution can be obtained with this same technique by using a combination of polycrystalline Be and powder graphite, which restricts E_f to $\lesssim 1.8$ meV. Since E_f is quite small, we have that $Q\approx k_i$, and we see that the wave vector and energy transfer are directly coupled. This also means that Q^2/ω is a constant in Eq. (2), and hence to a good approximation the observed intensity is directly related to the GDOS. With this technique a pyrolytic graphite PG(002) monochromator was employed for energy transfers $\lesssim 40$ meV, and we used collimations of 20′-20′ before and after the monochromator. For the range of higher-energy transfers (34–120 MeV), a Cu(220) monochromator was employed, with 40′-40′ collimation. In the low-energy regime (0–20 meV), where the measured Q becomes small for the filter-detector technique, we supplemented these data with data taken with the conventional triple-axis technique. In the triple-axis arrangement, E_f was fixed to 28 meV by use of a graphite analyzer, and measurements were made by the constant-Q technique for $3<Q<6$ Å^{-1} (see Table I). The procedure for determining the GDOS by the triple-axis method includes averaging the data taken with different Q values to average out any coherency effects. The data were also corrected for $\lambda/2$ contamination in the incident beam. The triple-axis measurements were taken on the BT-2 and BT-4 triple-axis spectrometers at NIST, with collimations of 60′-40′-20′-40′ with a Cu(220) monochromator or 40′-40′-40′-40′ with a PG(002) monochromator.

In order to identify possible weak crystal-field peaks in the scattering spectrum, we supplemented the filter-detector method with the time-of-flight (TOF) technique, where the Q dependence of the scattering can be used to differentiate phonon scattering ($\propto Q^2$) from the magnetic scattering which is proportional to the square of the magnetic form factor $f(Q)$. The time-of-flight data were obtained with the low-resolution-medium-energy chopper spectrometer (LRMECS) at the Intense Pulsed Neutron Source (IPNS) at Argonne National Laboratory. In the TOF technique, monochromatic neutrons are incident on the sample and the scattering at various energy transfers are obtained through their time of flight from the sample position to the 28 detector groups which span a range from $-7°$ to 117° with respect to the incident beam. Calibration of the ^{3}He detectors was made using scattering from a vanadium standard. The data reduction procedure involves averaging over a range of Q values, again to average out any coherency effects.[27] For energy transfers $\lesssim 40$ meV, neutrons with incident energy $E_i=50$ meV were used, while for higher-energy transfers neutrons with incident energy $E_i=130$ meV were employed. The various instrumental configurations are summarized in Table I along with some typical energy resolutions.

Data were obtained on polycrystalline samples of $Nd_{1.85}Ce_{0.15}CuO_4$, Nd_2CuO_4, Pr_2CuO_4, and $Pr_{1.85}Ce_{0.15}CuO_4$ weighing ~47, ~10, ~40, and ~40 g, respectively. All the samples were prepared by the usual methods.[28,29] The samples were encased in a rectangular Al can with dimensions $10\times5\times0.11$ cm^3 for the TOF experiments, whereas a sample can of size $4.5\times4.5\times0.69$ cm^3 was used for the filter-detector method experiments. Measurements were made at a temperature of 18 K at IPNS using a closed-cycle helium displex refrigerator and at a temperature of 4.2 K at NIST with a ^{4}He cryostat. Low temperatures were necessary to avoid scattering originating from transitions between crystal-field excited states. For both methods, corresponding background runs were taken with an empty Al can at the sample position. In addition to the background correction, data were also corrected for multiphonon contributions which were approximated by self-convoluting the phonon features in the spectrum. The result of this convolution is a featureless profile which increases approximately linearly up to an energy transfer well above the phonon cutoff frequency. Thus correction for the multiphonon contribution was made by subtracting from the background-corrected data a linear function which is ex-

TABLE I. Instrumental configurations used for the inelastic-neutron-scattering experiments and the corresponding resolutions. TOF, time of flight; Be, Be-graphite-Be filter; T, triple axis; PG, pyrolytic graphite (002) monochromator; Cu, Cu(220) monochromator.

No.	Mode	Collimations	E_i (meV)	E_f (meV)	Energy resolutions (meV)
1	TOF		50		2.5 at $E=36$ meV
2	TOF		130		3.2 at $E=93$ meV
3	Be-PG	20′-20′		~1	1.7 at $E=18$ meV
4	Be-Cu	40′-40′		~1	4.3 at $E=93$ meV
5	T-PG	40′-40′-40′-40′		28[a]	3.3 at $E=10$ meV
6	T-Cu	60′-40′-20′-40′		28[a]	1.7 at $E=10$ meV

[a]PG(002) analyzer.

trapolated from scattering at an energy well above the phonon cutoff frequency.

III. RESULTS AND DISCUSSION

The spectra obtained with the filter-detector method are shown in Fig. 1, with an expanded view displayed in Fig. 2, for the $Nd_{1.85}Ce_{0.15}CuO_4$ (top), $Pr_{1.85}Ce_{0.15}CuO_4$ (middle), and Pr_2CuO_4 (bottom) systems. All the data shown were corrected for background and multiphonon contributions as explained in the previous section. The peaks that are readily observed in Fig. 1 are those originating from ground-state crystal-field excitations. For the $Nd_{1.85}Ce_{0.15}CuO_4$ spectrum, a sharp crystal-field peak at 20.7 meV and another broader excitation at 26.4 meV can be clearly seen in the top of Fig.1. We have also taken a limited set of measurements on Nd_2CuO_4, where we found that these two crystal-field peaks are shifted by less than 1 meV to higher energies.[7] The crystal-field peak at ~26 meV in the $Nd_{1.85}Ce_{0.15}CuO_4$ system has a width that is considerably broader than the width of the same peak in the parent Nd_2CuO_4 system, and this broadening is likely caused by the random substitution of Ce, affecting the crystal-field environment. There are also crystal-field levels at energies 93 and 13 meV, which can be seen in the top of Fig. 2. Both these peaks have widths that are somewhat larger than the instrumental energy resolution. There is no single-phonon GDOS scattering above 83 meV, and therefore the peak at ~93 meV is due to purely magnetic scattering. The peak at 13 meV, on the other hand, has both magnetic and phonon contributions as we will show below when we present the TOF data.

For the Pr_2CuO_4 system, two crystal-field peaks are easily observed at 18.6 meV (bottom of Fig. 1) and at 87.9 meV (bottom of Fig. 2), in agreement with previous reported results.[21,22] However, these data have been taken with higher resolution than previous measurements. The peak at 18.6 meV has a resolution-limited width of 1.5 meV, and we note that it is much stronger than the peak at 87.9 meV. Recalling that Q varies with ΔE for the filter-detector method, we anticipate a reduction in intensity at the higher energies due to the decreasing magnetic form factor, but this only accounts for a factor of 3 in this case. We also note a small shoulder at ~22 meV, which originates from the ~88-meV crystal-field excitation via $\lambda/2$ contamination of the incident beam at this energy. We remark that generally $\lambda/2$ contamination is only a problem for energy transfers below $\lesssim 30$ meV and then only in cases where there is a strong excitation at high energies.

It can be seen from the figures that the crystal-field peaks in the Pr_2CuO_4 system undergo broadening and splitting when the system is doped with Ce to form $Pr_{1.85}Ce_{0.15}CuO_4$. The peak at 18.6 meV broadens and splits into peaks at 15 and 17.9 meV, and the peak at ~88 meV appears to split into two peaks at 81 and ~88 meV (middle of Fig. 2). All of the observed crystal-field peaks in our data are summarized in Table II and are in good agreement with those reported by other groups.[21–23] Although various groups agree on the observed crystal-field excitations, the proposed detailed crystal-field level schemes are subject to different interpretations.[21–23]

Figure 2, which is an enlargement of Fig. 1, illustrates the phonon scattering of interest. The phonon spectrum is rich in structure, as might be expected since these systems contain a large number of branches (21). There has also been substantial dispersion observed in many phonon branches, as, for example, in Nd_2CuO_4 where the dispersion relations have been measured in considerable detail.[15] Indeed, we note that there is little correspondence between the observed peaks in the GDOS and the excitations observed via Raman scattering or IR absorption.[7] In the top figure, the $Nd_{1.85}Ce_{0.15}CuO_4$ phonon density of states is seen to extend up to an energy of 83 meV, followed by a broad crystal-field peak at ~93 meV. In the energy region from ~17 to 30 meV, the phonon scattering is masked by the strong crystal-field peaks. Outside this region, the spectrum contains obvious peaks at energies ~13 and ~36 meV. We remark that we observed a background peak at ~36 meV due to the Al phonon density of states from the sample holder, and we have taken care to avoid "overcorrecting" this contribution by taking into account the sample absorption factor at this energy. The rest of the GDOS spectrum contains small peaks at ~42 and 52 meV, which sit on top of a broader peak, followed by another broad peak around 64 meV. There are shoulders at energies ~72 and ~78 meV before reaching the cutoff frequency.

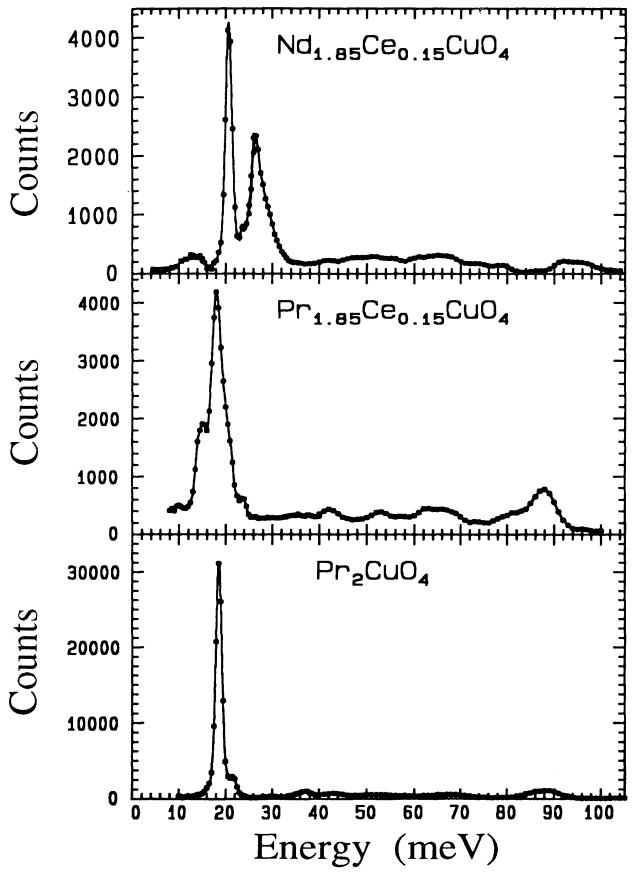

FIG. 1. Top portion of the figure shows the magnetic Nd^{3+} crystal-field scattering for the $Nd_{1.85}Ce_{0.15}CuO_4$ system at energies of 20.7 and 26.4 meV. The bottom portion of the figure shows the Pr^{3+} crystal-field peaks at 18.6 and 87.9 meV for the Pr_2CuO_4 system. These peaks split and broaden as the system is doped to form superconducting $Pr_{1.85}Ce_{0.15}CuO_4$ (middle). All of the above spectra were taken using the filter-detector method and have been corrected for background and multiphonon contributions.

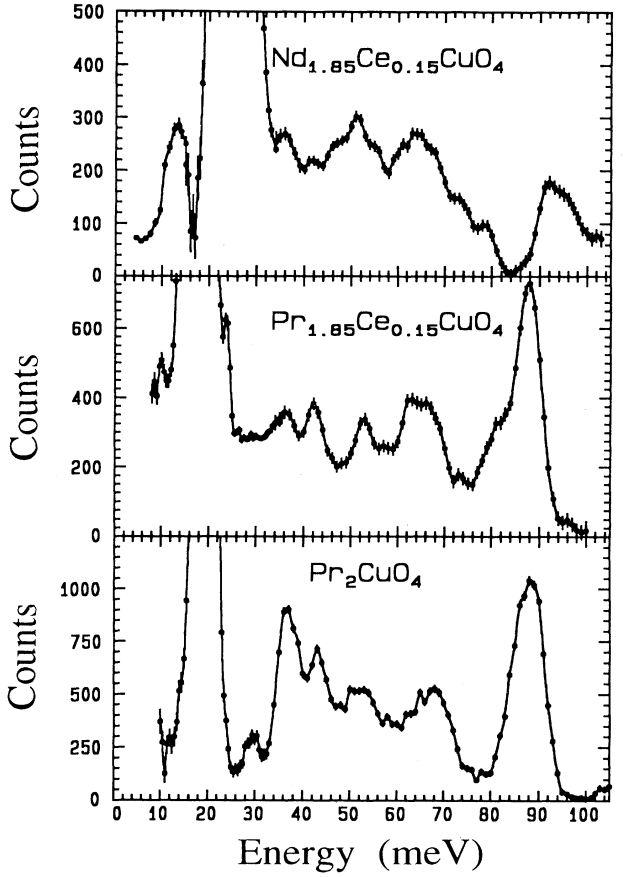

FIG. 2. Same data as in Fig. 1, plotted on a scale where the generalized phonon density of states (GDOS) can be observed. The peaks at ~93 meV in the top figure and at ~88 meV in the middle and bottom are magnetic crystal-field peaks. The peak at 13 meV in the $Nd_{1.85}Ce_{0.15}CuO_4$ spectrum contains contributions from both magnetic and phonon scattering.

The GDOS spectrum for the $Pr_{1.85}Ce_{0.15}CuO_4$ system shown in the middle of Fig. 2 appears to be somewhat different than the $Nd_{1.85}Ce_{0.15}CuO_4$ system despite their being isostructural. These differences cannot be attributed to the change in the scattering length for the rare-earth alloys as most of the rare-earth vibrational modes occur in the region below 30 meV owing to the heavy masses of the rare-earth ions.[30,15] The difference between the two GDOS spectra consists primarily in changes of the intensities of some structures, without apparent shifts in the energies. The peaks at 36 and 42 meV in $Pr_{1.85}Ce_{0.15}CuO_4$ have different relative intensities compared to the corresponding peaks observed in the $Nd_{1.85}Ce_{0.15}CuO_4$ spectrum. The broad feature at ~52 meV observed in the $Nd_{1.85}Ce_{0.15}CuO_4$ spectrum becomes a relatively sharp peak in the $Pr_{1.85}Ce_{0.15}CuO_4$ spectrum. In the energy range of 58–76 meV, the two spectra are in general agreement. The precise phonon cutoff frequency in the $Pr_{1.85}Ce_{0.15}CuO_4$ cannot be determined since scattering above ~76 meV is dominated by the neighboring crystal-field peak.

For the Pr_2CuO_4 system, we observe a phonon peak at ~30 meV. The observation of this feature is only possible due to the sharpness of the crystal-field peak at ~18 meV; it is not possible to observe this feature in the $Pr_{1.85}Ce_{0.15}CuO_4$ sample. On the other hand, the relative

TABLE II. Observed energies for the crystal-field peaks in $Nd_{1.85}Ce_{0.15}CuO_4$, $Pr_{1.85}Ce_{0.15}CuO_4$, and Pr_2CuO_4 measured at a temperature of 4.2 K.

$Nd_{1.85}Ce_{0.15}CuO_4$ E_{obs} (meV)	$Pr_{1.85}Ce_{0.15}CuO_4$ E_{obs} (meV)	Pr_2CuO_4 E_{obs} (meV)
13.0±0.4	15.0±0.4	18.6±0.2
20.7±0.2	17.9±0.4	
26.4±0.2	81.0±1.0	
93.1±0.4	87.9±0.4	87.9±0.4

intensities of the various structures of the GDOS spectrum in $Pr_{1.85}Ce_{0.15}CuO_4$ change substantially in intensity, particularly in the energy region of 33–63 meV; there are no dramatic shifts in the energies of phonon structures between the two spectra. In the Pr_2CuO_4 spectrum, the peak around 52 meV is broader (and perhaps split) than the corresponding peak in the $Pr_{1.85}Ce_{0.15}CuO_4$ spectrum. The peaks at 36 and 42 meV have higher intensities relative to the peak intensity at 52 meV in Pr_2CuO_4, whereas in the $Pr_{1.85}Ce_{0.15}CuO_4$ spectrum the peaks at 36, 42, and 52 meV have comparable peak intensities. Interestingly enough, the peak at 36 meV in the Pr_2CuO_4 spectrum has an intensity which is greater than any of the density-of-states features and is in fact comparable to the 88-meV crystal-field peak. This raises the question of whether this peak has a magnetic contribution, but we will see below that the TOF data rule out this possibility. Hence this scattering likely originates from oxygen vibrations.

The GDOS spectra obtained by TOF spectroscopy in the energy region 30–100 meV are shown in Fig. 3. The open circles are the TOF results, and the solid circles are the data obtained with the filter-detector method, shown for comparison. The top part of the figure represents the $Pr_{1.85}Ce_{0.15}CuO_4$ data, and the bottom part represents the data for $Nd_{1.85}Ce_{0.15}CuO_4$. These TOF data were taken with an incident energy $E_i = 130$ meV and have been averaged over a series of scans with Q values ranging from 5 to 10 Å^{-1}. In normalizing the averaged TOF scans to the filter data, we made use of the integrated intensities of the crystal-field peaks at the high end of the spectra after adjusting the factor $f^2(Q)$ to the value expected at the corresponding measured Q in the filter-detector data. It is important to note that in the TOF spectra the energy resolution coarsens as one measures toward lower energy, going from a resolution $\Delta E \cong 3.2$ meV at 93 meV to $\Delta E \cong 9.6$ meV at 36 meV. In the case of the filter-detector spectra, on the other hand, the resolution gets better, going from $\Delta E \cong 4.2$ meV at 93 meV to $\Delta E \cong 1.8$ meV at 36 meV. There is general agreement between the two sets of data for the $Pr_{1.85}Ce_{0.15}CuO_4$ spectrum, with the exception of the peak at 52 meV. This peak is clearly observed in the filter data, but not in the TOF data. The discrepancy at 52 meV may be due in part to the fact that the filter-detector method has ~3 times better resolution at this energy than the data taken by the TOF method. However, it may also be related to "coherency effects"; i.e., the data for the filter-detector method may not be averaging over a large enough range in Q. This effect would give rise to variations in the peak intensities as a function of Q, therefore affecting the relative intensities of the observed peaks in the filter data. Coherency effects are greatly reduced in the TOF technique since the data shown were obtained by averaging over a large range of Q. In the filter-detector method, the measured value for Q at 52 meV is 5.1 Å^{-1} and decreases down to $Q = 4.2$ Å^{-1} at 32 meV, which is still substantially larger than the size of the Brillouin zone (~2 Å^{-1}), yet the coherency effects may still be significant. The bottom of Fig. 3 compares the spectrum for $Nd_{1.85}Ce_{0.15}CuO_4$ between the TOF data and the filter data. Apart from the general agreement between the two spectra for energies $\gtrsim 55$ meV, there also appears to be a considerable difference in intensities between the two spectra for lower energies. For energies $\lesssim 55$ meV, features in the TOF spectrum have intensities larger than those observed in the filter data. This difference in intensities cannot be explained on the basis of energy resolutions alone in this energy range, as this would only mean that features seen in the filter data would not be well resolved in the TOF data. The investigation of the Q dependence of the scattering in the TOF method confirms the existence of phonon peaks at ~36 and ~42 meV as we will next show.

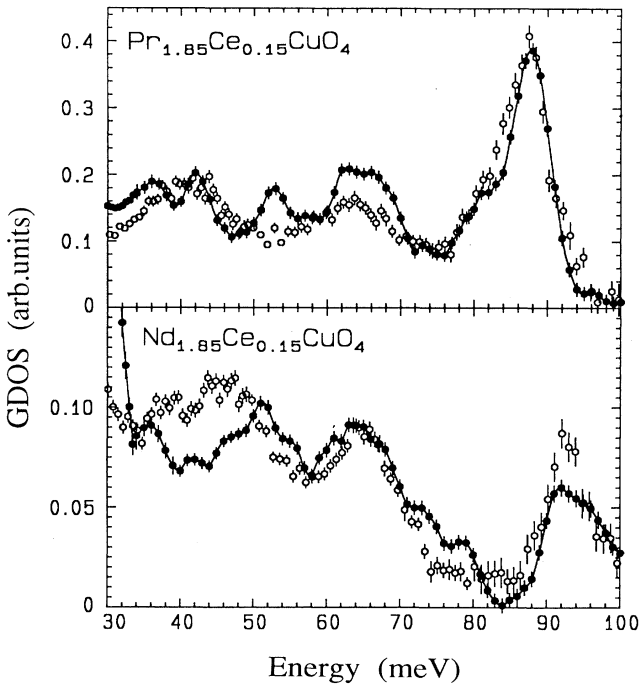

FIG. 3. Comparison of the generalized phonon density-of-states (GDOS) spectra taken by employing the filter-detector method (solid circles) with that taken using the time-of-flight spectrometer (open circles) for $Pr_{1.85}Ce_{0.15}CuO_4$ (top) and $Nd_{1.85}Ce_{0.15}CuO_4$ (bottom). The data for the time-of-flight method and the filter method were taken using instrumental configuration Nos. 2 and 4 from Table I, respectively. There is general agreement between the two methods except at 52 meV in the $Pr_{1.85}Ce_{0.15}CuO_4$ spectrum and in the lower-energy region in the $Nd_{1.85}Ce_{0.15}CuO_4$ spectrum (see text).

Figure 4 illustrates the variation of the integrated intensity as a function of Q obtained through the TOF method for peaks at energies of 13, 20.7, 26.4, and ~93 meV in the $Nd_{1.85}Ce_{0.15}CuO_4$ spectrum. The solid curve is a plot of the square of the form factor $f^2(Q)$ for the Nd^{3+} ion.[31] All the integrated intensities in Fig. 4 are scaled to unity at $Q = 0$ for comparison purposes. It can be seen from the figure that the 20.7-, 26.4-, and 93-meV peaks are indeed crystal-field peaks since they conform closely to $f^2(Q)$. At the highest Q values (> 9.25 Å^{-1}), the intensity of the 93-meV peak has decreased

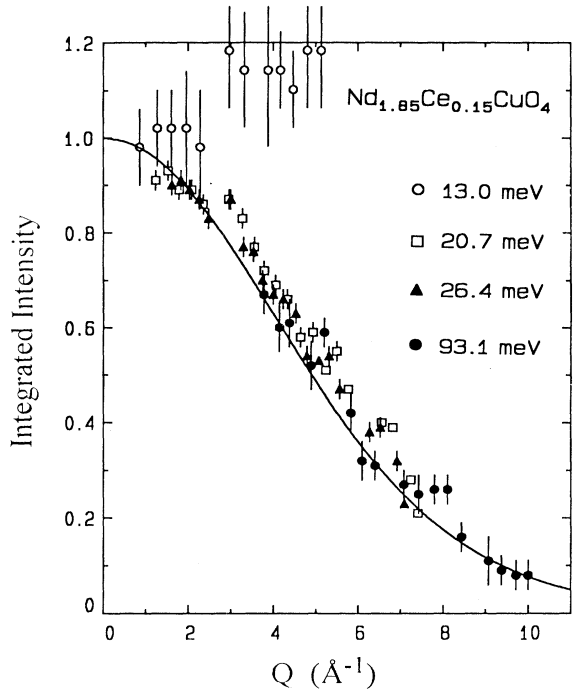

FIG. 4. Q dependence of the magnetic crystal-field integrated intensities for the $Nd_{1.85}Ce_{0.15}CuO_4$ system. For the crystal-field peaks at 20.7 meV (□), 26.4 meV (△), and 93.1 meV (●), the Q dependence of their intensities agrees well with the square of the magnetic form factor $f^2(Q)$ for Nd^{3+} (solid curve). However, the peak at 13 meV (○) increases in intensity with increasing Q, demonstrating that there is a phonon contribution at this energy.

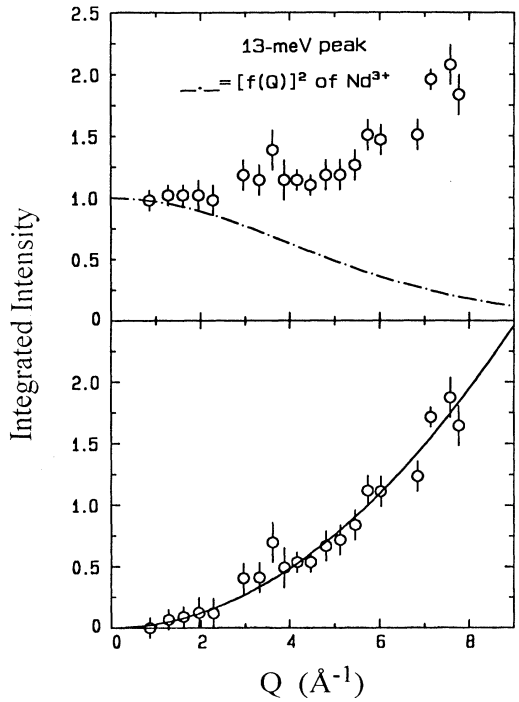

FIG. 5. Top portion of the figure shows the scattering intensity vs Q for 13-meV scattering in $Nd_{1.85}Ce_{0.15}CuO_4$. This scattering can be separated into a magnetic component at small Q, which follows the square of the Nd^{3+} magnetic form factor (dot-dashed curve), and a phonon contribution which varies as Q^2. The bottom portion of the figure shows the remainder of the scattering with the magnetic contribution removed and where we see that it follows the Q^2 dependence (solid curve) quite well.

significantly, allowing the determination and confirmation of the phonon cutoff frequency, which is at ~83 meV. Unfortunately, the intensities of the two other crystal-field peaks still dominate the scattering in the 18–32-meV region even at the highest measured Q values, prohibiting the determination of the phonon spectrum in this particular energy region.

For the case of the peak at 13 meV, it can be seen from the figure that its intensity has an upward trend with increasing Q, which is better illustrated in the top of Fig. 5, where the Q dependence of the integrated intensity is plotted for the 13-meV peak only. Also plotted on the top of Fig. 5 is $f^2(Q)$ (dot-dashed curve) for Nd^{3+}. It is clear that this peak contains both magnetic and phonon scattering. At small Q the magnetic scattering is strongest, while the phonon scattering ($\propto Q^2$) dominates the magnetic part for high values of Q. This is better illustrated in the bottom of Fig. 5 where the contribution from the magnetic scattering, which is approximated by $f^2(Q)$ in the top of Fig. 5, has been subtracted from the total peak intensity, giving a result of a plot of only phonon intensity versus Q. We see that we obtain a nice separation of the magnetic and phonon scattering; the phonon character of the scattering at 13 meV is confirmed by the fact that the subtracted intensity conforms to the Q^2 behavior, which is depicted as the solid curve in the bottom of Fig. 5.

Figure 6 shows a plot of the scattering function $S(Q,\omega)$ versus energy for three values of Q, in the energy region around 36 meV. All the data shown have been corrected for background contributions. The top figure is scattering associated with $Q=2.73$ Å^{-1}, and in this energy region obviously the spectrum is flat; the extra scattering around 31 meV comes from the shoulder of the neighboring crystal-field peak. In the middle figure where scattering is shown for $Q=5.23$ Å^{-1}, increases in intensities can be seen in the 33–38-meV region developing into some structure. The structure eventually develops into a peak around 36 meV, which is observed in the highest-angle (and therefore highest-Q) detectors, as shown in the bottom figure for $Q=6.34$ Å^{-1}. Thus in spite of the fact that the 36-meV peak is only observed for the few highest Q values, the increasing trend in intensities is confirmation of a peak in the GDOS at this energy. We have also confirmed the presence of a phonon peak at 42 meV by the same analysis. In fact, the same observations have been done on other parts of the spectrum with the result that the energy region below 18 meV and from 30 meV up to the phonon cutoff frequency the scattering is lattice dynamical in origin. We cannot establish the character of the small peak at ~52 meV seen in the filter

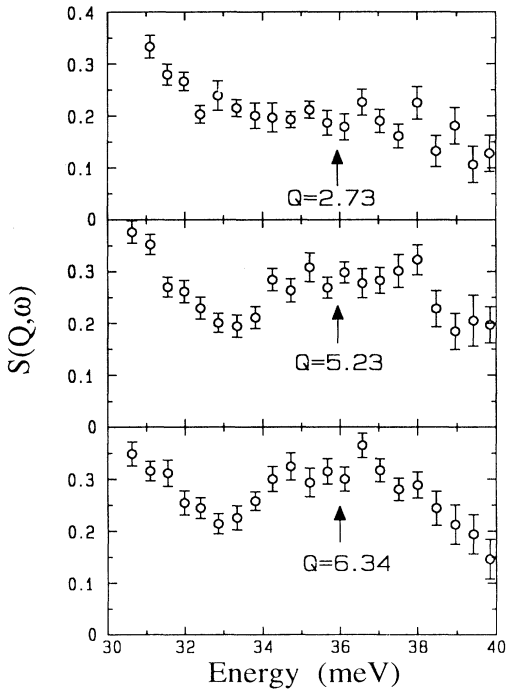

FIG. 6. TOF data showing the Q dependence of the scattering at 36 meV for the $Nd_{1.85}Ce_{0.15}CuO_4$ system. The increase in scattering with increasing Q demonstrates that this is phonon scattering.

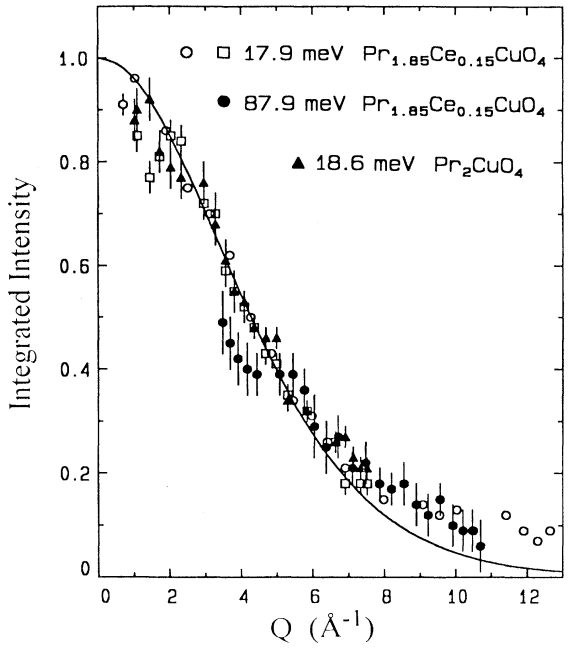

FIG. 7. Q dependence of the integrated intensities for the crystal-field transitions in the $Pr_{1.85}Ce_{0.15}CuO_4$ system. The data symbolized by (○) and (●) represent the peaks at 17.9 and 87.9 meV, respectively, while the data symbolized by (□) and (△) represent the 18.6-meV peak for the Pr_2CuO_4 system. The Q dependence of the intensities of these peaks are in very good agreement with the square of the magnetic form factor for the Pr^{3+} ions (solid curve).

data by this means since it is not observable in the TOF data. However, neutron-scattering[14] and infrared measurements[30] reveal the existence of a zone-center mode energy at ~52 meV, which suggest that the observed peak at this energy in the filter data might be a phonon peak.

For the $Pr_{1.85}Ce_{0.15}CuO_4$ and Pr_2CuO_4 samples, the Q dependence of the integrated intensities of the crystal-field peaks are shown in Fig. 7 for peaks at energies 18 and ~88 meV. The behavior of these intensities with Q confirms that these peaks are indeed Pr^{3+} crystal-field peaks since the data yields good agreement with $f^2(Q)$ for Pr^{3+} ions.[31] Unfortunately, even for the highest Q measured, the peak around 88 meV in both samples still contains substantial magnetic intensity, preventing a good determination of the phonon cutoff frequency. However, in analogy with the $Nd_{1.85}Ce_{0.15}CuO_4$ density of states, we expect that the phonon cutoff frequency to be somewhere between 80 and 90 meV.

To identify the origin of the peak at 36 meV in Pr_2CuO_4, we analyzed the Q dependence of its intensity as depicted in the top of Fig. 8, while the same analysis for the 30-meV peak is illustrated in the bottom of Fig. 8 for $3.5 < Q < 7$ Å^{-1}. The solid curves shown are functions proportional to Q^2, and this describes the general behavior of both peak intensities as a function of Q, showing that both peaks contain scattering which originates mainly from phonons. We have also determined the existence of these two phonon peaks in superconducting $Pr_{1.85}Ce_{0.15}CuO_4$ through the same procedure. The

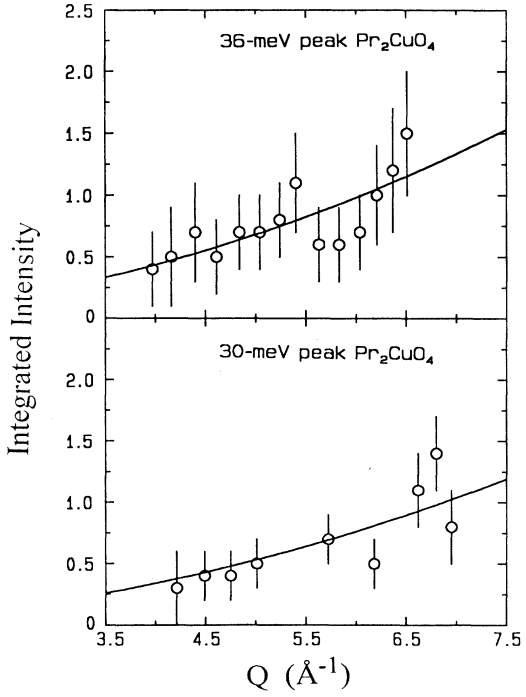

FIG. 8. Q dependence of the integrated intensities for phonon peaks at energies 36 meV (top) and 30 meV (bottom) for the Pr_2CuO_4 system. The solid curves are proportional to Q^2.

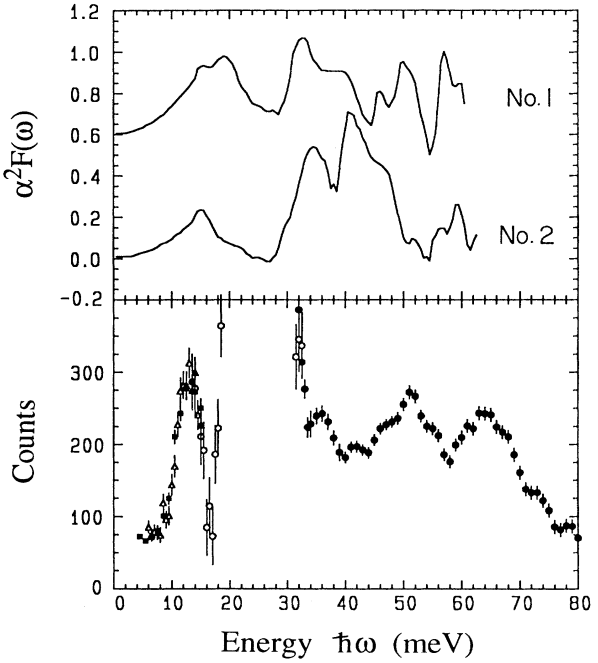

FIG. 9. Comparison of tunneling measurements of $\alpha^2F(\omega)$ (top) for two samples of $Nd_{1.85}Ce_{0.15}CuO_4$ (Ref. 11) with the generalized phonon density of states (bottom). There are substantial similarities between the two spectra at lower energies, as indicated by the presence of peaks at ~14, 36, and ~42 meV in both spectra.

scattering in the region of 52 meV may also be phonon in origin, but there is no clear peak observed in the TOF data. We note that infrared reflectivity measurements reveal a zone-center mode at this energy.[32]

Finally, we address the question of whether phonons may play a role in the electron-pairing mechanism in these materials by comparing the Eliashberg-coupling function $\alpha^2F(\omega)$ extracted from tunneling measurements with the GDOS. Figure 9 displays the spectra of $\alpha^2F(\omega)$ for two samples (to convey the repeatability of the data) of $Nd_{1.85}Ce_{0.15}CuO_4$ obtained from tunneling measurements,[11] while the bottom part of the figure shows the phonon density-of-states GDOS for $Nd_{1.85}Ce_{0.15}CuO_4$ taken with the filter method. The peak at ~14 meV is in good agreement with the GDOS, as are the peaks at ~35 and ~40 meV. The correspondence with the neutron data at higher energies is not particularly good, but neither is the repeatability of the tunneling data, and indeed this is not surprising as the tunneling measurements are known to become less reliable with increasing energy.[2] To the extent that the comparison between the GDOS spectrum of $Nd_{1.85}Ce_{0.15}CuO_4$ and the corresponding tunneling spectrum is correct, this suggests that phonons are to some extent involved in the electron-pairing mechanism in these electron-doped superconductor systems. Since the measured GDOS in the $Pr_{1.85}Ce_{0.15}CuO_4$ system reveals a different shape in some of the structures than that of the $Nd_{1.85}Ce_{0.15}CuO_4$ system, it would be interesting to see how the GDOS of $Pr_{1.85}Ce_{0.15}CuO_4$ compares with the tunneling spectrum $\alpha^2F(\omega)$ of the $Pr_{1.85}Ce_{0.15}CuO_4$ system. Of course, the possibility that other excitations are also playing a role in the pairing cannot be ruled out.

In conventional superconductors the observation of substantial phonon softening, which is a shifting of the phonon modes toward lower energies, as the system goes into the superconducting state is taken as evidence of phonon involvement in the formation of superconductivity. Measurements of the GDOS in the related system $La_{2-x}Sr_xCuO_4$ have indicated some phonon softening when going into the superconducting state.[33] The softening occurs in the energy region of the oxygen-vibrational modes, yet the effect is believed to be too small to account for the high T_c values if conventional electron-phonon models are employed.[33] In our data, the comparison of the GDOS between the parent insulating Pr_2CuO_4 and the superconducting $Pr_{1.85}Ce_{0.15}CuO_4$ from Fig. 2 reveals no appreciable softening. Instead, as the system goes from $Pr_{1.85}Ce_{0.15}CuO_4$ to Pr_2CuO_4, substantial increases in intensities occur between the 33 and 63 meV. These changes likely entail a number of phonon branches and certainly in part result from the change in the screening in going from insulator to conductor. There may also be a magnetovibrational contribution[34] to the scattering in the insulating phase, where the Cu spins are ordered. This might affect the relative intensities of the phonon peaks. As for the differences in the shape of the GDOS spectrum between $Pr_{1.85}Ce_{0.15}CuO_4$ and $Nd_{1.85}Ce_{0.15}CuO_4$ below 60 meV, we can only speculate as to whether or not any phonon modes in this energy region are affected by the decrease in the stability of the T' structure as the rare-earth radius increases from Nd to Pr.[35] It would be useful to compare the GDOS with other $R_{1.85}Ce_{0.15}CuO_4$ systems for R=Sm,Gd, but these measurements are difficult to carry out due to the high neutron absorption cross section of these rare-earth ions.

ACKNOWLEDGMENTS

We would like to acknowledge helpful discussions with R. L. Greene and K. E. Gray. Two of us (I.W.S. and J.W.L.) would like to thank the staff of IPNS for their hospitality during our stay at Argonne. The research at Maryland is supported by the NSF, DMR Grant No. 89-21878, and by the Electric Power Research Institute and Baltimore Gas & Electric Co. Work performed at Argonne is supported by the U.S. DOE, Basic Energy Sciences under Contract No. W-31-109-ENG-38.

[1]For a general review of the oxide superconductors, see *High Temperature Superconductivity,* edited by J. W. Lynn (Springer-Verlag, New York, 1990).

[2]For a general review of phonon effects in superconductors, see P. B. Allen, in *Dynamical Properties of Solids,* edited by G. K. Horton and A. A. Maradudin (North-Holland, Amsterdam, 1980), Vol. 3.

[3]H. J. Bournemann, D. E. Morris, and H. B. Liu, Physica C **182,**

132 (1991).
[4]Y. Tokura, H. Takagi, and S. Uchida, Nature **337**, 334 (1989).
[5]B. Batlogg, S.-W. Cheong, G. A. Thomas, S. L. Cooper, L. W. Rupp, Jr., D. H. Rapkine, and A. S. Cooper, Physica C **185-189**, 1385 (1991).
[6]Ru and Zr are examples of conventional superconductors with no isotope effect; see C. Kittel, *Introduction to Solid State Physics,* 6th ed. (Wiley, New York, 1986), p. 330. Also see J. W. Garland, Jr., Phys. Rev. Lett. **11**, 111 (1963); **11**, 114 (1963).
[7]J. W. Lynn, I. W. Sumarlin, D. A. Neumann, J. J. Rush, J. L. Peng, and Z. Y. Li, Phys. Rev. Lett. **66**, 919 (1991).
[8]M. Arai, K. Yamada, Y. Hidaka, S. Itoh, Z. A. Bowden, A. D. Taylor, and Y. Endoh, Phys. Rev. Lett. **69**, 359 (1992).
[9]H. A. Mook, B. C. Chakoumakos, M. Mostoller, A. T. Boothroyd, and D. McK. Paul, Phys. Rev. Lett. **69**, 2272 (1992).
[10]For a review of tunneling data in the oxide systems, see J. R. Kirtley, Int. J. Mod. Phys. **4**, 201 (1990).
[11]Q. Huang, J. F. Zasadzinski, N. Tralshawala, K. E. Gray, D. G. Hinks, J. L. Peng, and R. L. Greene, Nature **347**, 369 (1990).
[12]D. G. Hinks, D. R. Richards, B. Dabrowski, D. T. Marx, and A. W. Mitchell, Nature **335**, 419 (1988).
[13]C.-K. Loong, P. Vashishta, R. K. Kalia, M. H. Degani, D. L. Price, J. D. Jorgensen, D. G. Hinks, B. Dabrowski, A. W. Mitchell, D. R. Richards, and Y. Zheng, Phys. Rev. Lett. **62**, 2628 (1989); C.-K. Loong, P. Vashishta, R. K. Kalia, Wei Jin, M. H. Degani, D. G. Hinks, D. L. Price, J. D. Jorgensen, B. Dabrowski, A. W. Mitchell, D. R. Richards, and Y. Zheng, Phys. Rev. B **45**, 8052 (1992).
[14]L. Pintschovius, N. Pyka, W. Reichardt, A. Yu. Rumiantsev, N. L. Mitrofanov, A. S. Ivanov, G. Collin, and P. Bourges, Physica C **185-189**, 156 (1991).
[15]A. S. Ivanov, N. L. Mitranov, A. Yu. Rumiantsev, L. Pintschovius, N. Pyka, and W. Reichardt, Fiz. Nizk. Temp. [Sov. J. Low Temp. Phys. **17**, 693 (1991)].
[16]J. W. Lynn, I. W. Sumarlin, S. Skanthakumar, W.-H. Li, R. N. Shelton, J. L. Peng, Z. Fisk, and S.-W. Cheong, Phys. Rev. B **41**, 2569 (1990).
[17]M. Matsuda, K. Yamada, K. Kakurai, H. Kadowaki, T. R. Thurston, Y. Endoh, Y. Hidaka, R. J. Birgeneau, M. A. Kastner, P. M. Gehring, A. H. Moudden, and G. Shirane, Phys. Rev. B **42**, 10098 (1990).
[18]S. Skanthakumar, J. W. Lynn, J. L. Peng, and Z. Y. Li, J. Magn. Magn. Mater. **104-107**, 519 (1992).
[19]S. Skanthakumar, H. Zhang, T. W. Clinton, I. W. Sumarlin, W.-H. Li, and J. W. Lynn, J. Appl. Phys. **67**, 4530 (1990).
[20]The spin-wave velocity has recently been measured to be $\sim$700 meV Å in Pr_2CuO_4; see I. W. Sumarlin, J. W. Lynn, T. Chattopadhyay, S. N. Barilo, and D. I. Zhigunov (private communication).
[21]A. T. Boothroyd, S. M. Doyle, D. McK. Paul, and R. Osborn, Phys. Rev. B **45**, 10075 (1992), and references therein.
[22]P. Allenspach, A. Furrer, R. Osborn, and A. D. Taylor, Z. Phys. B **85**, 301 (1991).
[23]P. Hoffmann, M. Loewenhaupt, S. Horn, P. v. Aaken, and H.-D. Jostarndt, Physica B **163**, 271 (1990); V. Nekvasil, Physica C **170**, 469 (1990).
[24]I. W. Sumarlin, J. W. Lynn, D. A. Neumann, J. J. Rush, J. L. Peng, Z. Y. Li, and S. J. Hagen, Physica C **185-189**, 2571 (1991).
[25]P. F. Miceli, S. E. Youngquist, D. A. Neumann, and H. Zabel, Phys. Rev. B **34**, 8977 (1986); see also V. S. Oskotskii, Fiz. Tverd. Tela (Leningrad) [Sov. Phys. Solid State **9**, 420 (1967)].
[26]F. Gompf, H. Lau, W. Reichardt, and J. Salagado, in *Proceedings of the International Conference on Inelastic Scattering of Neutrons, Grenoble, 1972* (IAEA, Vienna, 1972), p. 137.
[27]For detailed data reduction in the time-of-flight experiment, see N. Lustig, J. S. Lannin, J. M. Carpenter, and R. Hasegawa, Phys. Rev. B **32**, 2778 (1985).
[28]J. L. Peng, R. N. Shelton, and H. B. Radousky, Solid State Commun. **71**, 479 (1989).
[29]J. L. Peng and R. L. Greene, Physica C **172**, 143 (1990).
[30]For the zone-center mode assignment, see E. T. Heyen, G. Kliche, W. Kress, W. Kõnig, M. Cardona, E. Rampf, J. Prade, U. Schröder, A. D. Kulkarni, F. W. de Wette, S. Piñol, D. Mck. Paul, E. Morán, and M. A. Alario-Franco, Solid State Commun. **74**, 1299 (1990).
[31]M. Blume, A. J. Freeman, and R. E. Watson, J. Chem. Phys. **37**, 1245 (1962).
[32]M. K. Crawford, G. Burns, G. V. Chandrashekar, F. H. Dacol, W. E. Farneth, E. M. McCarron III, and R. J. Smalley, Solid State Commun. **73**, 507 (1990).
[33]B. Renker, F. Gompf, E. Gering, N. Nücker, D. Ewert, W. Reichardt, and H. Rietschel, Z. Phys. B **67**, 15 (1987).
[34]S. W. Lovesey, *Theory of Thermal Neutron Scattering* (Oxford University Press, New York, 1984), Vol. 2, p. 35.
[35]Y. Y. Xue, P. H. Hor, R. L. Meng, Y. K. Tao, Y. Y. Sun, Z. J. Huang, L. Gao, and C. W. Chu, Physica C **165**, 357 (1990).